Pharm Res (2015) 32:2538–2547
DOI 10.1007/s11095-015-1642-1

RESEARCH PAPER

Quantitative Evaluation of mMate1 Function Based on Minimally Invasive Measurement of Tissue Concentration Using PET with [^{11}C]Metformin in Mouse

Tomotaka Shingaki • W. Ewan Hume • Tadayuki Takashima • Yumiko Katayama • Takashi Okauchi • Emi Hayashinaka • Yasuhiro Wada • Yilong Cui • Hiroyuki Kusuhara • Yuichi Sugiyama • Yasuyoshi Watanabe

Received: 31 October 2014 / Accepted: 27 January 2015 / Published online: 27 February 2015

ABSTRACT

Purpose To evaluate the function of multidrug and toxin extrusion proteins (MATEs) using ^{11}C-labeled metformin ([^{11}C]metformin) by positron emission tomography (PET).

Methods PET was performed by intravenous bolus injection of [^{11}C]metformin. Pyrimethamine at 0.5 and 5 mg/kg was intravenously administered to mice 30 min prior to the scan. Integration plot analysis was conducted for calculating liver ($CL_{uptake,liver}$), kidney ($CL_{uptake,kidney}$) tissue uptake, intrinsic biliary ($CL_{int,bile}$) and urinary ($CL_{int,urine}$) excretion clearances of [^{11}C]metformin.

Results Visualization by PET showed that pyrimethamine increased concentrations of [^{11}C]metformin in the liver and kidneys, and decreased the concentrations in the urinary bladder without changing the blood profiles. Pyrimethamine had no effect on the $CL_{uptake,liver}$ and $CL_{uptake,kidney}$, which were similar to the blood-flow rate. $CL_{int,bile}$ with regard to the liver concentration was unable to be determined, but administration of 0.5 and 5 mg/kg of pyrimethamine increased the liver-to-blood ratio to 1.6 and 2.3-fold, respectively, indicating that pyrimethamine inhibited the efflux of [^{11}C]metformin from the liver. $CL_{int,urine}$ with regard to the corticomedullary region concentrations was decreased 37 and 68% of the control by administration of 0.5 and 5 mg/kg of pyrimethamine, respectively ($P < 0.05$).

Conclusions Tissue concentration based investigations using [^{11}C]metformin by PET enables the functional analysis of MATEs in the liver and kidneys.

KEY WORDS Drug-drug interactions (DDIs) · Metformin · Multidrug and toxin extrusion proteins (Mates) · Organic cation transporters (Octs) · Positron emission tomography (PET)

ABBREVIATIONS

AUC	The area under the concentration-time curve
$CL_{int,bile\ or\ urine}$	The intrinsic bile or urinary excretion clearances
CL_{renal}	The renal clearance
CL_{tot}	The total body clearance
$CL_{uptake,organ}$	The uptake clearance in the liver or kidney
MATEs	Human multidrug and toxin extrusion proteins
mMates	Mouse multidrug and toxin extrusion proteins
OCTs	Human organic cation transporters
mOcts	Mouse organic cation transporters
PET	Positron emission tomography
ROIs	Regions of interest
V_E	Extravascular space volume
VOIs	Volumetric regions of interest

INTRODUCTION

Metformin is an orally bioavailable biguanide medicament widely used as an insulin sensitizer in the treatment of type 2 diabetes targeting the liver and resulting in the inhibition of

Electronic supplementary material The online version of this article (doi:10.1007/s11095-015-1642-1) contains supplementary material, which is available to authorized users.

T. Shingaki • W. E. Hume • Y. Katayama • T. Okauchi • E. Hayashinaka • Y. Wada • Y. Cui • Y. Watanabe (✉)
RIKEN Center for Life Science Technologies, 6-7-3 Minatojima-minamimachi, Chuo-ku, Kobe, Hyogo 650-0047, Japan
e-mail: yywata@riken.jp

T. Takashima
RIKEN Center for Molecular Imaging Sciences, Where Reorganized to RIKEN Center for Life Science Technologies, Chuo-ku, Kobe, Hyogo 650-0047, Japan

H. Kusuhara
Laboratory of Molecular Pharmacokinetics, Graduate School of Pharmaceutical Sciences, The University of Tokyo, 7-3-1 Hongo, Bunkyo-ku, Tokyo 113-0033, Japan

Y. Sugiyama
Sugiyama Laboratory, RIKEN Innovation Center, Yokohama Bio Industry Center, 1-6 Suehiro-cho, Tsurumi-ku, Yokohama, Kanagawa 230-0045, Japan

gluconeogenesis and activation of AMP activated protein kinase. Organic cation transporter-1 (OCT1) and multidrug and toxin extrusion protein-1 (MATE1) account for the hepatic uptake and subsequent canalicular efflux of hydrophilic metformin [1–6]. The major elimination pathway of metformin from the systemic circulation is urinary excretion which involves tubular secretion mediated by OCT2 and MATEs [7, 8]. Unlike the liver, two MATE isoforms (MATE1 and MATE2-K) are considered to mediate the efflux of metformin in the kidneys [9–13].

Genetic polymorphisms, and drug-drug interactions (DDIs) are known to cause inter-individual differences in the pharmacokinetics of metformin, and thereby, the response to metformin. OCT1 variants are associated with inter-individual differences in the disposition of metformin, and its glucose lowering effects in the oral glucose tolerance test [5], whereas OCT2 variants are associated with inter-individual difference in the renal clearance [14]. MATE1 variants have a greater glucose-lowering response [15] than that on the pharmacokinetics of metformin [16], whereas MATE2-K promoter variants oppositely reduce the pharmacological effects of metformin as a result of affecting the pharmacokinetic mechanism [16]. Drugs that inhibit MATEs at their clinically relevant doses, and thereby, causing DDIs in the urinary excretion include cimetidine, pyrimethamine and trimethoprim [3, 17, 18]. It is difficult from a practical point of view to investigate these interactions by conventional pharmacokinetic analysis because of the low contribution of hepatic elimination to the systemic elimination. Furthermore, given that the uptake process is the rate-determining process in the overall hepatobiliary transport and tubular secretion, variation in the efflux activity of MATEs caused by the DDIs or by genetic factors could show a greater impact on the tissue concentrations than on the plasma concentrations [19]. Therefore, minimally invasive methods which can measure the tissue concentrations of drugs should be established for better understanding of the hepatobiliary and tubular secretion of metformin.

Positron emission tomography (PET) enables minimally invasive analysis of drug concentrations in tissues with high sensitivity and good spatio-temporal resolution, allowing direct measurement of the intra-tissue distribution of drugs [20]. We have established several PET probes for studying drug transporters and demonstrated the usefulness of these probes in pharmacokinetic and DDI studies in animals and humans, such as [^{11}C]dehydropravastatin and (15*R*)-16-m-[^{11}C]tolyl-17,18,19,20-tetranorisocarbacyclin methyl ester ((15*R*-)-[^{11}C]TIC-Me) for OATP1B1 and multidrug resistance-associated protein 2 (MRP2) [21–24], [^{11}C]telmisartan for OATP1B3 [25], [^{11}C]SC-62807 for breast cancer resistance protein (BCRP) [26], and R-[^{11}C]verapamil and [^{11}C]oseltamivir for P-glycoproteins (P-gp) [27]. Because of negligible metabolism in the body and the specificity of the organic cation transporters, metformin was considered to be a promising probe for investigating OCTs and MATEs. We were able to successfully develop [^{11}C]metformin as a new PET probe [28].

Here, we used PET to visually determine the tissue uptake and subsequent efflux clearances of [^{11}C]metformin in the liver and kidney that relate to the transport activities of mOcts and mMate1 in mice pretreated with pyrimethamine, a potent inhibitor of MATE1 [2]. We demonstrated the pharmacokinetics of [^{11}C]metformin as a PET probe for analysis of the hepatic and renal organic cation transport systems based on the tissue concentrations.

MATERIALS AND METHODS

Materials

Metformin was purchased from Alexis Biochemicals (San Diego, CA, USA). [^{11}C]Metformin in Fig. 1 was synthesized according to a procedure reported previously [28]. The radiochemical and chemical purities of [^{11}C]metformin were assessed by high-performance liquid chromatography and were found to be greater than 99.7±0.6% and 78.0±18.4%, respectively. The purified fraction was recovered in approximately 4 mL of 40 mM ammonium acetate. The specific radioactivity was 6.18±4.08 GBq/μmol at the time of injection. Pyrimethamine was purchased from MP Biomedicals (Santa Ana, CA, USA).

Animals

Male ddY mice weighing 32–36 g (6–7 weeks old; n=3–4 for each set of experiments) were purchased from Japan SLC Inc. (Hamamatsu, Shizuoka, Japan). All experimental protocols were approved by Ethics Committee on Animal Care and Use of RIKEN Center for Life Science Technologies and were performed in accordance with the Principles of Laboratory Animal Care (NIH publication no. 85–23, revised 1985).

PET Scans

All PET scans were performed as described previously using a microPET Focus220 scanner (Siemens, Knoxville, TN, USA)

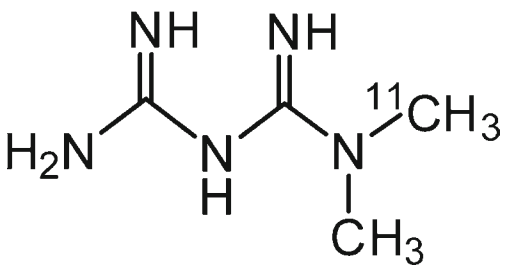

Fig. 1 Chemical structure of [^{11}C]metformin.

designed for laboratory animals [28]. Briefly, mice were kept anesthetized with a mixture of 1.5% isoflurane and nitrous oxide:oxygen (7:3); their body temperature was maintained at 37°C and they were placed on the PET scanner gantry. At the start of the emission scan, [^{11}C]metformin was administered as a single bolus *via* the tail vein within 1–2 s at a dose of 171 ± 64 MBq/kg in 150–200 μL of 40 mM ammonium acetate. The chemical amount of [^{11}C]metformin for the intravenous bolus injection was calculated as 1.42 ± 0.58 nmol/body (0.18 ± 0.07 μg/body).

For the functional analysis of mOcts and mMate1, at 30 min before the administration of [^{11}C]metformin, mice were given an intravenous bolus injection of 0.5 or 5 mg/kg of pyrimethamine, which was dissolved at a concentration of 0.1 or 1.0 mg/mL in saline containing a mixture of 5% ethanol and 5% polyoxyethylene [20] sorbitan monooleate (Tween 80). Control mice received an intravenous injection of vehicle alone. An emission scan was performed for 30 min and sorted into 26 dynamic sinograms according to the following sequence: 12 × 5 s, 3 × 20 s, 3 × 60 s, 5 × 120 s, and 3 × 300 s.

Analysis of PET Imaging Data

PET images were reconstructed using Siemens microPET manager 2.4.1.1 by Fourier Rebinning and standard 2D filtered back projection using a Ramp filter with a cut-off at the Nyquist frequency. Regions of interest (ROIs) were automatically defined on the right ventricle, liver, kidneys, and urinary bladder using the isocontouring tool in the PMOD program (ver. 3.3, PMOD Technologies Ltd., Zurich, Switzerland), as described previously [22]. Briefly, ROIs were automatically drawn on tissue images at each frame in which these tissues could be easily identified. The defined ROIs were then manually corrected by fitting the images of each tissue slice and time frame without overlapping any of the defined ROIs. All ROIs were combined and changed to volumetric regions of interest (VOIs). In this study, the kidneys were subdivided into two regions, the renal pelvis and corticomedullary regions. The VOIs of the pelvis were defined at around frame #20 (500 s), during which the radioactivity migrated to the pelvis. The VOIs for the corticomedullary region were defined at around frame #6 (30 s) with several spheres on the region external of the pelvis in both kidneys (Fig. 2). Time-radioactivity curves for each tissue and region were constructed by normalizing decay-corrected time-radioactivity measurements to the injected activity (% IA) of [^{11}C]metformin.

Analysis of Blood Samples

Samples of venous blood were collected from mice at 5, 15, and 30 min, and the radioactivity in blood was measured by a 1470 Wizard Automatic Gamma Counter (PerkinElmer Life and Analytical Sciences, Waltham, MA, USA). Consistent with our previous investigation [28], no radioactive metabolites of [^{11}C]metformin were observed in the urine, blood, or liver homogenates, indicating that [^{11}C]metformin did not

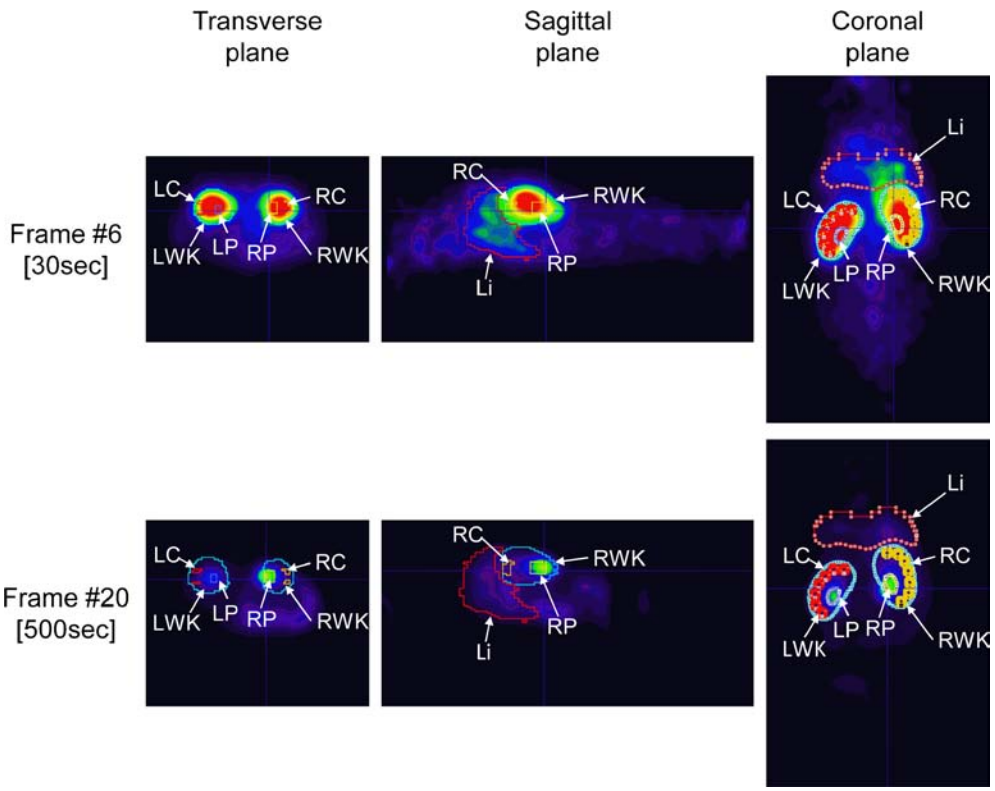

Fig. 2 Identification of the renal pelvis and corticomedullary regions in the kidney on PET images after intravenous bolus administration of [^{11}C]metformin to mice. Representative transverse, sagittal, and coronal plane of PET images in the abdominal region of mice after intravenous bolus administration of [^{11}C]metformin. Images of frame #6 and 20 corresponds to 30 and 500 s after administration, respectively. RC and LC, right and left corticomedullary regions; RP and LP, right and left pelvis; RWK and LWK, right and left whole kidney; Li, liver.

undergo any metabolism or degradation in the experimental mice and that the radioactivity obtained from the PET imaging data represented [^{11}C]metformin [28]. The radioactivity in blood was compared to that obtained from the PET imaging data analysis on the right ventricle. Time-radioactivity curves for right ventricle was well fit to the radioactivity in blood counted by gamma-counter (Supplemental Fig. 1). The curves were fitted by 2-compartent model and the calculated value was used for the kinetic analysis. The blood sample in the pyrimethamine-pretreatment group at the end of the PET scan was determined the plasma pyrimethamine concentration. Plasma samples were mixed with a 5-fold volume of acetonitrile and centrifuged at 14,000 rpm for 2 min at 4°C. The resulting supernatants were evaporated, reconstituted with mobile phase, and then analyzed by liquid chromatography/mass spectrometry (Thermo Scientific, San Jose, CA, USA).

Kinetic Analysis

The total body clearance ($CL_{tot,blood}$) and the renal clearance with respect to the blood concentration ($CL_{renal,blood}$) were calculated using the following equations:

$$CL_{tot,blood} = Dose/AUC_{0-30,blood}$$
$$CL_{renal,blood} = X_{30,urine}/AUC_{0-30,blood}$$

where Dose and $X_{30,urine}$ represent the radioactivity amount of [^{11}C]metformin administered and that associated with urinary bladder from 0 to 30 min, respectively. $AUC_{0-30,blood}$ represents the area under the radioactivity-time curve in the right ventricle fitted by 2-compartment model as blood profile.

The liver and kidney uptake clearances of [^{11}C]metformin ($CL_{uptake,liver}$ and $CL_{uptake,kidney}$) was estimated by the integration plot method [23] using the VOIs in the liver and corticomedullary region of the kidney and the radioactivity curves in the right ventricle encompassing approximately 5–45 s in the liver and 10–50 s in the corticomedullary region of the kidney in the linear range of the plot after [^{11}C]metformin administration. Values for both CL_{uptake} were calculated using the following equation:

$$X_{t,organ}/C_{t,blood} = CL_{uptake} \times AUC_{0-t,blood}/C_{t,blood} + V_E$$

where $X_{t,organ}$ represents the amount of radioactivity per g tissue in the liver or corticomedullary region of the kidney at time *t*, as determined by PET imaging data analysis. $C_{t,blood}$ represents the concentration of radioactivity in the right ventricle fitted by 2-compartment model as blood profile at time *t*, as determined by PET imaging data analysis. CL_{uptake} represents the uptake clearance of [^{11}C]metformin in the liver or kidney, and $AUC_{0\text{-}t,blood}$ represents the area under the radioactivity-time curve in the right ventricle fitted by 2-compartment model as blood profile from time 0 to time *t*. The CL_{uptake} value can be obtained from the linear part of the slope at the beginning of the plot of $X_{t,organ}/C_{t,blood}$ *versus* $AUC_{0\text{-}t,blood}/C_{t,blood}$. V_E is calculated as the y-intercept of the integration plot.

The intrinsic urinary excretion clearance of [^{11}C]metformin in the kidney ($CL_{int,urine}$) was also estimated by the integration plot method [26] using the corticomedullary region of kidney and time-radioactivity curves in the urinary bladder encompassing 45 s–6 min in the linear range of the plot after [^{11}C]metformin administration. Values for $CL_{int,urine}$ were calculated using the following equation:

$$X_{t,urine} = CL_{int,urine} \times AUC_{0-t,corticomedulla} + V_E$$

where $X_{t,urine}$ represents the amount of radioactivity in the urinary bladder at time *t*, as determined by PET image analysis. $CL_{int,urine}$ represents the intrinsic urinary excretion clearance of [^{11}C]metformin in the kidney, and $AUC_{0\text{-}t,corticomedulla}$ represents the area under the radioactivity-time curve in the corticomedullary region of kidney from time 0 to time *t*. The $CL_{int,urine}$ value can be obtained from the slope of the plot of $X_{t,urine}$ *versus* $AUC_{0\text{-}t,corticomedulla}$. V_E is calculated as the y-intercept of the integration plot.

Statistical Analysis

All values are presented as the mean ± SD. Ordinary one-way ANOVA was used for comparisons. In the case of significant differences, post hoc Tukey's multiple comparisons test with a single pooled variance were performed. Differences were considered significant at $P<0.05$.

RESULTS

Distribution of Radioactivity in the Abdominal Region After Intravenous Administration of [^{11}C]Metformin

Maximum intensity projection PET images of the distribution of radioactivity in the abdominal region after intravenous administration of [^{11}C]metformin with or without pyrimethamine pretreatment are shown in Fig. 3. The radioactivity determined in this study was associated with unmetabolized [^{11}C]metformin, since [^{11}C]metformin does not undergo any biotransformations in mice [28]. In control mice (Fig. 3a), the majority of the radioactivity was detected in the liver, kidneys, and urinary bladder at 2 min postadministration. Subsequently, the radioactivity increased in the urinary bladder while the radioactivity in the kidneys, liver, and intestine gradually

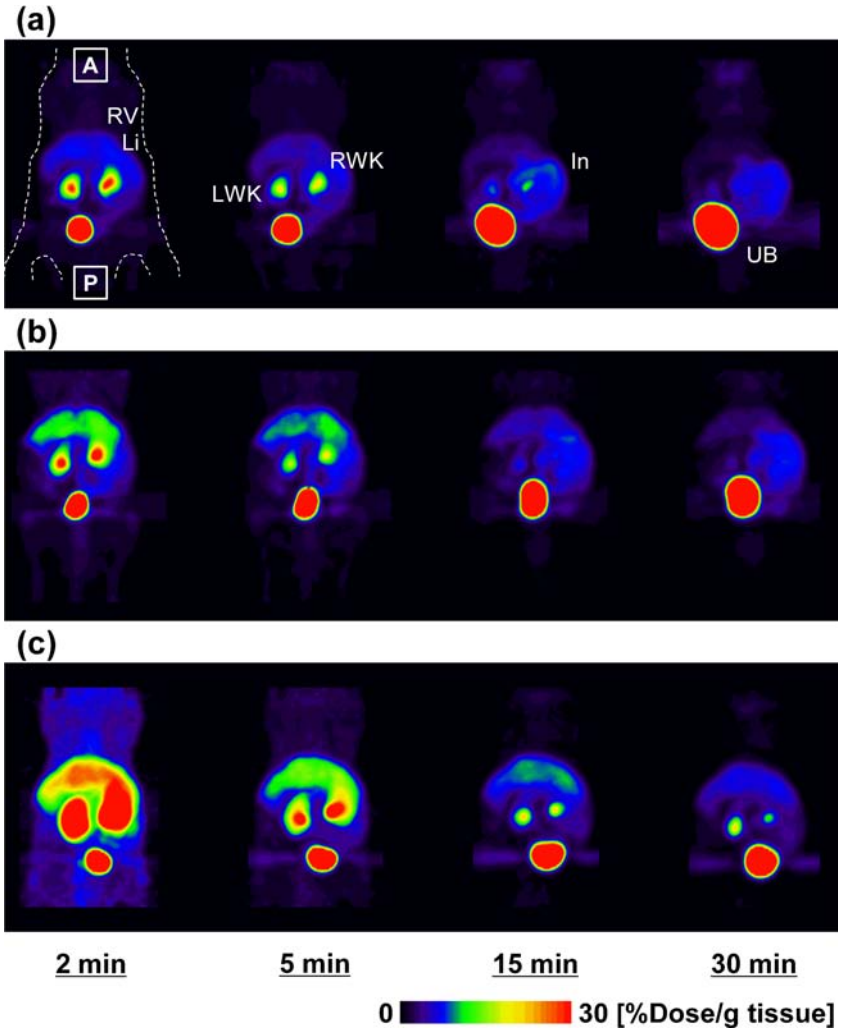

Fig. 3 Color-coded PET images of the abdominal region of mice after intravenous bolus administration of [^{11}C]metformin. Representative coronal maximum intensity projection PET images of radioactivity in the abdominal region of mice after intravenous bolus administration of [^{11}C]metformin. Images were captured at 2, 5, 15, and 30 min in (**a**) control mice and mice pretreated with (**b**) 0.5 and (**c**) 5 mg/kg of pyrimethamine. *A*, anterior direction; *P*, posterior direction; *RV*, right ventricle; *Li*, liver; *LWK*, left whole kidney; *RWK*, right whole kidney; *In*, intestine; *UB*, urinary bladder.

decreased until the end of the scan. Pyrimethamine increased the retention of radioactivity in the kidneys and liver in a dose-dependent manner, whereas it decreased the level of radioactivity in the urinary bladder (Fig. 3b and c). The plasma concentrations of pyrimethamine during the PET scan were 0.38 ± 0.25 and 3.7 ± 1.2 μM with pyrimethamine doses of 0.5 and 5 mg/kg at the end of experiment (30 min), respectively, by liquid chromatography-mass spectrometry analysis. Taking the unbound fraction of pyrimethamine in plasma (8.1%, [2]) into consideration, the corresponding unbound concentrations were 0.031 and 0.3 μM, the levels which are similar to or above the K_i value for mMate1 (0.04 μM) but below the K_i values for mOct1/2 (3–6 μM) [2].

Quantitative Biodistribution Profiles of [^{11}C]Metformin in Mice

Time-radioactivity curves in the right ventricle fitted using a 2-compartment model showed that pyrimethamine did not affect the concentration of [^{11}C]metformin in the blood (Fig. 4a), total body clearance ($CL_{tot,blood}$) and the area under the time-radioactivity profiles (AUC) in blood (Table I). The data was comparable to the radioactivity in blood samples determined by gamma-counter (Supplemental Fig. 1). In contrast, pretreatment with pyrimethamine resulted in a decrease in the cumulative radioactivity in the urine, which was estimated from the PET imaging data by examining VOIs on the urinary bladder (Fig. 4b), between control mice and mice treated with 5 mg/kg pyrimethamine ($P<0.05$). The renal clearance ($CL_{renal,blood}$) was slightly decreased by treatment of pyrimethamine, with no significance (Table I).

Time-radioactivity curves in the liver are shown in Fig. 5a. Pyrimethamine increased the concentration profiles of [^{11}C]metformin dose dependently, and the AUC in the liver showed significance between control mice and mice treated with 0.5 and 5 mg/kg pyrimethamine ($P<0.01$ and 0.001), respectively (Table I). Time-radioactivity curves in the whole kidney are shown in Fig. 5b. Pyrimethamine increased the concentration profiles of [^{11}C]metformin with similar degree on both treatments. Histologically, the kidney consists of a

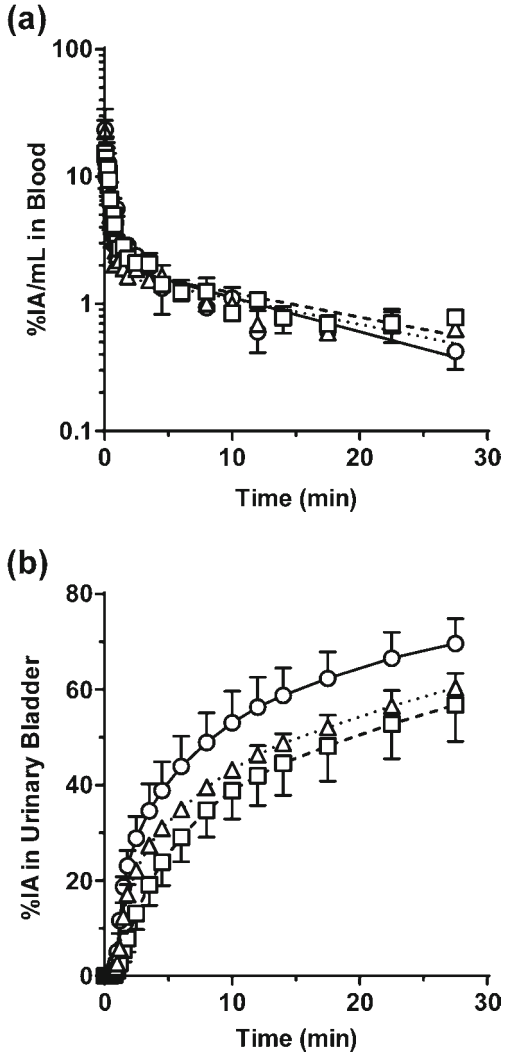

Fig. 4 Blood and urinary bladder content time-radioactivity curves determined after intravenous bolus administration of [^{11}C]metformin to mice. Total radioactivity profiles were determined 30 min after mice received an intravenous bolus administration of [^{11}C]metformin. Profiles for the (**a**) right ventricle as blood and (**b**) urinary bladder were determined by PET imaging analysis ($n=3$, 4 and 3 in control mice and mice treated with 0.5 and 5 mg/kg of pyrimethamine, respectively). Symbols represent control (*open circles*) mice and mice treated with 0.5 and 5 mg/kg of pyrimethamine (*open triangles and squares*, *respectively*) 30 min prior to PET scanning. A solid, dotted, and broken line on the blood profiles describes the fitting line using 2-compartment model in control mice and mice treated with 0.5 and 5 mg/kg of pyrimethamine, respectively.

Table I Pharmacokinetic Parameters Obtained by PET

	Control ($n=3$)	Pyrimethamine	
		0.5 mg/kg ($n=4$)	5 mg/kg ($n=3$)
$AUC_{0-30,blood}$ (%Dose·min/mL)	36 ± 2	33 ± 5	37 ± 2
$CL_{tot,blood}$ (mL/min/kg)	84 ± 7	94 ± 16	79 ± 7
$X_{0-30,urine}$ (%Dose)	70 ± 5	60 ± 3	57 ± 8 *
$CL_{renal,blood}$ (mL/min/kg)	59 ± 9	57 ± 7	45 ± 9
$AUC_{0-30,liver}$ (%Dose·min/g tissue)	60 ± 9	120 ± 14 **	146 ± 13 ***
$AUC_{0-30,corticomedula}$ (%Dose·min/g tissue)	86 ± 16	150 ± 19 *	205 ± 42 **
$CL_{uptake,liver}$ (mL/min/kg)	61 ± 0.6	58 ± 16	57 ± 6
(mL/min/g tissue)	1.1 ± 0.03	1.1 ± 0.3	1.0 ± 0.2
$V_{E,liver}$ (mL/kg)	7.1 ± 6.0	8.5 ± 5.5	4.4 ± 5.8
$X_{30,liver}/C_{30,blood}$ (mL/g tissue)	2.7 ± 1.5	4.3 ± 1.0	6.1 ± 1.8
$CL_{uptake,kidney}$ (mL/min/kg)	45 ± 11	60 ± 22	48 ± 14
(mL/min/g tissue)	3.1 ± 0.6	3.9 ± 0.9	3.0 ± 0.7
$V_{E,kidney}$ (mL/kg)	5.9 ± 7.3	5.1 ± 6.2	6.2 ± 6.6
$X_{30,corticomedulla}/C_{30,blood}$ (mL/g tissue)	2.9 ± 1.6	6.4 ± 2.4	7.0 ± 2.1
$CL_{int,urine}$ (mL/min/kg)	38 ± 7	24 ± 2 **	12 ± 3 *** †

*, **, ***; $P<0.05$, 0.01, and 0.001 to control mice, respectively

†; $P<0.05$ to mice pretreated by 0.5 mg/kg pyrimethamine

The conversion of $CL_{uptake,organ}$ in mL/min/kg was calculated from the $CL_{uptake,organ}$ in mL/min/g tissue multiplying by actual tissue weight (g) at the end of the assay and dividing the body weight of mice (kg)

number of complex components. Therefore, the renal regions were defined further by analyzing separately the corticomedullary region and the renal pelvis. The cortex and the medulla, collectively referred to as the corticomedullary region, are external to the pelvis, and the pelvis, located in the central region of the kidney, is involved in collecting the urine. The radioactivity in the corticomedullary region of the kidney showed a low deviation compared with the whole kidney. Moreover, as compared with the control group, pretreatment with pyrimethamine led to a dose-dependent elevation in the radioactivity in the corticomedullary region of the kidney (Fig. 5c). The AUC in the corticomedullary region of the kidney showed significance between control mice and mice treated with 0.5 and 5 mg/kg pyrimethamine ($P<0.05$ and 0.01), respectively (Table I). In contrast, a large deviation in time-radioactivity curve values were observed for the pelvis (Fig. 5d). Most of the radioactivity profiles of [^{11}C]metformin in the pelvis could be associated with the urine shown a large deviation.

Pharmacokinetic Analysis of PET Imaging Data for the Liver and Kidney Uptake and Urinary Excretion of [^{11}C]Metformin in Mice

Integration plots were drawn to calculate the liver uptake ($CL_{uptake,liver}$), kidney uptake ($CL_{uptake,kidney}$) and intrinsic urinary excretion ($CL_{int,urine}$) clearances of [^{11}C]metformin, which represent the uptake and intrinsic efflux activity across the basal and apical membrane in the liver and corticomedullary region of the kidney, respectively (Fig. 6). The $CL_{uptake,liver}$ and extracellular volume in the liver ($V_{E,liver}$) values at the beginning of the plot were similar among groups

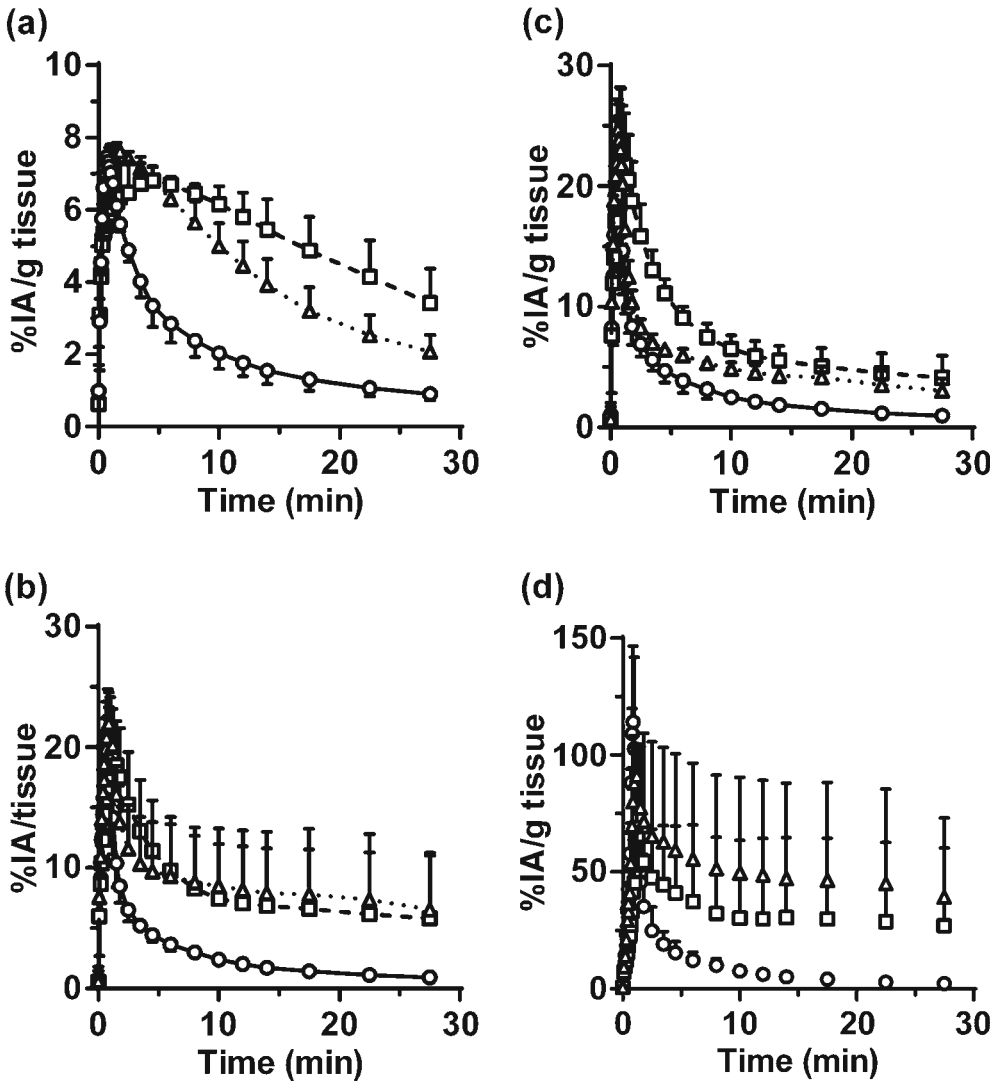

Fig. 5 Time-radioactivity curves in the liver and kidney determined after intravenous bolus administration of [^{11}C]metformin. Total radioactivity profiles for the (**a**) liver and (**b**) whole kidney, (**c**) corticomedullary region and (**d**) renal pelvis of the kidneys were determined by PET imaging analysis 30 min after mice received an intravenous bolus administration of [^{11}C]metformin. Symbols represent control ($n=3$; open circles) mice and mice treated with 0.5 and 5 mg/kg of pyrimethamine ($n=4$ and 3; open triangles and squares, respectively) 30 min prior to PET scanning.

and the $CL_{uptake,liver}$ were nearly two-thirds of the hepatic blood flow rate in mice (90 mL/min/kg) [29]. When the integration plot for the liver was kept drawing until 30 min of the end of the assay, the plot reached the plateau. The X_{liver}/C_{blood} at 30 min was increased by the treatment of 0.5 and 5 mg/kg pyrimethamine (Fig. 6a and Table I).

The $CL_{uptake,kidney}$ values and extracellular volume of the corticomedullary region in the kidney ($V_{E,corticomedulla}$) at the beginning of the plot were also similar among groups and closed to the renal blood flow rate in mice (65 mL/min/kg) [29]. The $CL_{uptake,kidney}$ per kg was similar to the $CL_{uptake,liver}$ per kg in each group. But the $CL_{uptake,kidney}$ per g tissue was approximately 3-fold higher than the $CL_{uptake,liver}$ per g tissue in each group. The profile of $X_{corticomedulla}/C_{blood}$ at 30 min was increased by the treatment of 0.5 and 5 mg/kg pyrimethamine, and the profiles were different from that in the liver and slightly inclined at the end of the assay (30 min) (Fig. 6b and Table I).

In $CL_{int,urine}$, the pretreatment with 0.5 mg/kg of pyrimethamine resulted in decreases of 37% in the $CL_{int,urine}$ to control mice ($P<0.01$). That with 5 mg/kg of pyrimethamine decreased of 68% in the $CL_{int,urine}$ to control mice ($P<0.001$). The decrease in the $CL_{int,urine}$ in mice between pretreated with 0.5 and 5 mg/kg of pyrimethamine was also significant ($P<0.05$) (Fig. 6c and Table I).

DISCUSSION

We assessed the tissue concentration-based pharmacokinetics of [^{11}C]metformin for analysis of the hepatic and renal organic cation transport system, particularly that involving mOcts and mMate1, by PET in mouse as feasibility study for future clinical study.

The biodistribution of [^{11}C]metformin in mice, by PET, shows extensive localization in the bladder followed by the

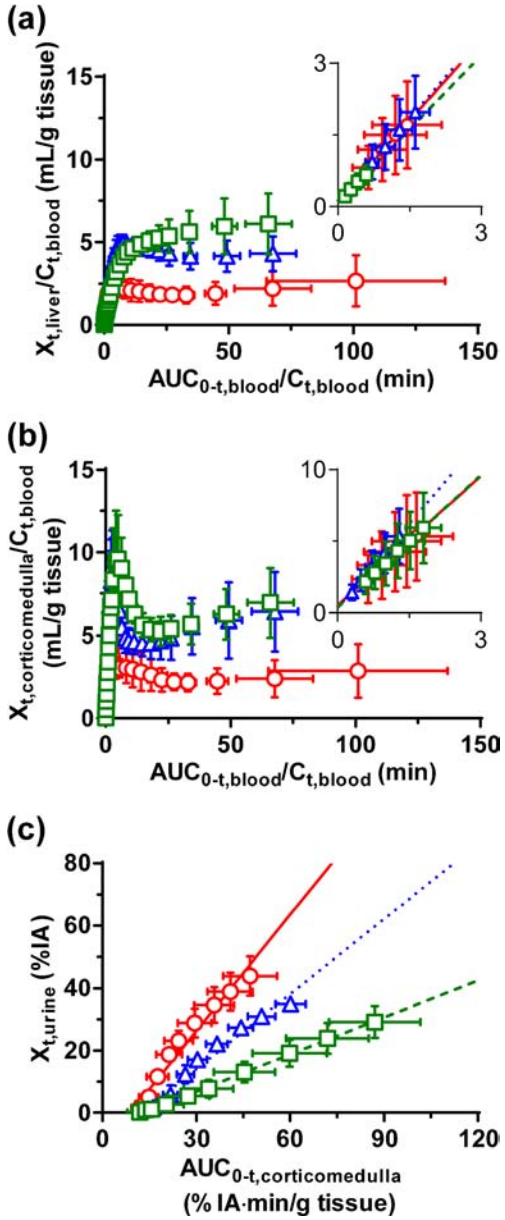

Fig. 6 Integration plot analysis of the liver and kidney after intravenous bolus administration of [^{11}C]metformin in mice. Integration plots after mice received an intravenous bolus administration of [^{11}C]metformin were constructed for the uptake clearance in the (**a**) liver, and (**b**) corticomedullary region of the kidney to the end of the assay. Inset Fig. 6a and b describes the early phase of the plot between 5–45, and 10–50 s, respectively. (**c**) The intrinsic urinary excretion clearance using integration plot analysis were constructed by the corticomedullary region of the left and right kidneys and the cumulative radioactivity in the contents of the urinary bladder. Symbols represent control (n = 3; circles in red) mice and mice treated with 0.5 and 5 mg/kg of pyrimethamine (n = 4 and 3; triangles in blue and squares in green, respectively) 30 min prior to PET scanning.

kidney, and to lesser degree to the liver (Fig. 3). Pyrimethamine increased the concentrations of [^{11}C]metformin both in the liver and kidneys and decreased that in the urinary bladder in a dose dependent manner (Fig. 3). Blood concentrations of [^{11}C]metformin shows bi-phasic disappearance; rapid elimination from the systemic circulation for 1 min after the intravenous bolus injection (Fig. 4a). The fraction of [^{11}C]metformin that accumulated in the urinary bladder during 30 min was similar to that recovered into the urine 60 min after intravenous bolus injection of non-radiolabeled metformin [30], supporting that the amount of [^{11}C]metformin in the urinary bladder is regarded as that excreted into the urine. Pyrimethamine showed only a negligible effect on the blood concentrations, whereas the amount excreted into the bladder was only slightly decreased. Consequently, the $CL_{renal,blood}$ was unchanged by pyrimethamine administration (Table I). The concentrations in the liver and kidney reached maximum values shortly after the injection (Fig. 5a and b). Pyrimethamine did not affect the maximum concentrations of [^{11}C]metformin in the liver and kidney, but clearly prolonged the retention probably due to the decline of the net efflux process in these organs.

To determine the tissue uptake and subsequent efflux clearances, integration plot analysis was conducted using the PET imaging data. The CL_{uptake} of [^{11}C]metformin in the liver and kidneys indicates the activities of mOcts. These were similar to their own organ blood-flow rates, indicating extensive tissue uptake activities both in the liver and kidney, and this parameter was not affected by pyrimethamine. The intrinsic biliary excretion clearance of [^{11}C]metformin with regard to the liver concentration was unable to be estimated because of the low radioactivity associated with gall bladder and small intestine; however, the fact that pyrimethamine increased the liver-to-blood ratio, indicates the net efflux of [^{11}C]metformin from the liver was significantly inhibited by pyrimethamine. In contrast, the intrinsic urinary excretion clearance ($CL_{int,urine}$) of [^{11}C]metformin could be determined, and it was significantly decreased by pyrimethamine, indicating a significant inhibition of the efflux of [^{11}C]metformin mediated by mMate1 in the kidney.

The initial % of injected activity per unit tissue weight in the corticomedullary region of the kidney (17–28% within 2 min) was approximately 3-fold higher than that in the liver (6–8% within 5 min) (Fig. 5a and c), and that the $CL_{uptake,kidney}$ per g tissue was also approximately 3-fold higher than the $CL_{uptake,liver}$ per g tissue (Table I). Because of the difference in the tissue size, $CL_{uptake,liver}$ (per body) was similar to $CL_{uptake,kidney}$ in the body. Notably, $CL_{uptake,liver}$ (per body) was similar to the blood flow rate despite the negligible contribution of biliary excretion into the bile (<1%) [2]. Thus, metformin may undergo significant sinusoidal efflux in the liver. In fact, Zamek-Gliszczynski *et al.* reported that metformin preloaded into the liver was mainly secreted into the out flow by *in situ* liver perfusion [31]. The effect of pyrimethamine on the liver concentrations of metformin may involve an inhibition of sinusoidal efflux as well as canalicular efflux.

The variance in the accumulation of radioactivity in the kidney in Fig. 5b occurred in the region that likely corresponds

to the renal pelvis, where the urine is temporarily concentrated. Including the radioactivity in this region will lead to an overestimation of the actual radioactivity subjected to uptake into the kidney or efflux into the urine. We therefore assigned VOIs for the corticomedullary region and pelvis separately in the subsequent analyses (Fig. 5c and d). The resulting time profiles of radioactivity in the kidneys were clearly differentiated between the pyrimethamine pretreatment groups, in which the AUCs in mice pretreated with 0.5 and 5.0 mg/kg of pyrimethamine resulted in increases of 74 and 138% to control mice ($P<0.05$ and 0.01 in 0.5 and 5.0 mg/kg of pyrimethamine, respectively). For the quantitative integration plot analysis for mMate1 activity in the kidney, the $CL_{int,urine}$ was defined using the sum of the AUCs for the left and right corticomedullary regions, because the cumulative radioactivity associated with the urinary bladder represents the total radioactivity excreted from the left and right kidneys. The $CL_{int,urine}$ significantly decreased along with an increasing pyrimethamine dose (Fig. 6c and Table I). The moderate inhibition of mMate1 observed following pretreatment with pyrimethamine at a dose of 0.5 mg/kg is consistent with our previous estimation (63% inhibition) [2]. Pretreatment with 5.0 mg/kg of pyrimethamine decreased $CL_{int,urine}$ to 32% of that in control mice. Ito *et al.* reported that the amount of metformin excreted into the urine by glomerular filtration was approximately 30%, accounting for minor fraction of the net urinary excretion [2]. Based on the renal clearance of metformin and the glomerular filtration rate, giving a 5 mg/kg of pyrimethamine to mice might fully inhibit (32% to control mice) the mMate1 activity at the renal tubules. Clinical PET study may enable the estimation of the function of MATEs in the kidneys in more detail, since the regions in the kidneys are able to be identified easily due to the organ size.

Compounds that interact with mMate1 could affect the tissue concentrations of drugs to a greater degree than they affect the blood concentrations (Fig. 5), thereby enhancing the drug's effect when targets are located intracellularly. The pharmacological target tissue of metformin is the liver where OCT1 and MATE1 determine its pharmacological effect [1–6]. Genetic factors of OCT1 and MATE1 have been reported that influence the pharmacokinetics and pharmacodynamics [16]; however, we lack quantitative information of their *in vivo* effect on the hepatobiliary transport formed by OCT1 and MATE1 in humans. Moreover, the nephrotoxic effect of cisplatin was enhanced in mice when mMate1 is inhibited by pyrimethamine [32]. As the measurement of plasma concentrations and urinary excretion is insufficient, a minimally invasive method for measuring tissue concentrations, such as PET, would be highly valuable in enhancing our understanding of the pharmacokinetic factors underlying interindividual differences in drug responses. Clinical studies using [^{11}C]metformin would also contribute to better understanding the factors causing interindividual differences in hepatobiliary transport.

In the present study, the inhibition of mMate1, rather than inhibition of mOct2, was actually the underlying mechanism, as we hypothesized [33]. It is believed that inhibition of basolateral uptake by OCT2 is the mechanism underlying drug interactions involving cimetidine. In fact, as the renal clearance of metformin is blood-flow limited [2], it precludes the evaluation of basolateral uptake activity in this study, although in humans, the CL_{renal} of metformin is not blood-flow limited [4, 34]. [^{11}C]Metformin will therefore enable the investigation of the basolateral uptake process mediated by OCT2 in humans, and a clinical PET study using [^{11}C]metformin may provide concrete evidence supporting our hypothesis. In conclusion, we have demonstrated that a minimally invasive and an intracellular concentration-based PET imaging analyses with [^{11}C]metformin enables elucidation of the function of mMate1 in the kidney *in vivo*. [^{11}C]Metformin is a promising PET probe for evaluating the functions of OCTs and MATEs in future drug development and clinical studies.

ACKNOWLEDGMENTS

We thank Mr. Masahiro Kurahashi of Sumitomo Heavy Industry Accelerator Service Ltd. for operation of the cyclotron. This study was partly carried out as the Research Project for the "Establishment of Evolutional Drug Development with the Use of Microdose Clinical Trial" sponsored by the New Energy and Industrial Technology Development Organization. Part of this work was also supported by JSPS KAKE NHI Grant number 24229002.

Conflict of Interest The authors report no conflicts of interest.

REFERENCES

1. Wang DS, Jonker JW, Kato Y, Kusuhara H, Schinkel AH, Sugiyama Y. Involvement of organic cation transporter 1 in hepatic and intestinal distribution of metformin. J Pharmacol Exp Ther. 2002;302:510–5.
2. Ito S, Kusuhara H, Kuroiwa Y, Wu C, Moriyama Y, Inoue K, *et al.* Potent and specific inhibition of mMate1-mediated efflux of type I organic cations in the liver and kidney by pyrimethamine. J Pharmacol Exp Ther. 2010;333:341–50.
3. Kusuhara H, Ito S, Kumagai Y, Jiang M, Shiroshita T, Moriyama Y, *et al.* Effects of a MATE protein inhibitor, pyrimethamine, on the renal elimination of metformin at oral microdose and at therapeutic dose in healthy subjects. Clin Pharmacol Ther. 2011;89:837–44.
4. Wang ZJ, Yin OQ, Tomlinson B, Chow MS. OCT2 polymorphisms and in-vivo renal functional consequence: studies with metformin and cimetidine. Pharmacogenet Genomics. 2008;18:637–45.
5. Shu Y, Brown C, Castro RA, Shi RJ, Lin ET, Owen RP, *et al.* Effect of genetic variation in the organic cation transporter 1, OCT1, on metformin pharmacokinetics. Clin Pharmacol Ther. 2008;83:273–80.

6. Umehara KI, Iwatsubo T, Noguchi K, Kamimura H. Functional involvement of organic cation transporter1 (OCT1/Oct1) in the hepatic uptake of organic cations in humans and rats. Xenobiotica. 2007;37:818–31.
7. Hillgren KM, Keppler D, Zur AA, Giacomini KM, Stieger B, Cass CE, *et al.* Emerging transporters of clinical importance: an update from the International Transporter Consortium. Clin Pharmacol Ther. 2013;94:52–63.
8. Yonezawa A, Inui K. Importance of the multidrug and toxin extrusion MATE/SLC47A family to pharmacokinetics, pharmacodynamics/toxicodynamics and pharmacogenomics. Br J Pharmacol. 2011;164:1817–25.
9. Otsuka M, Matsumoto T, Morimoto R, Arioka S, Omote H, Moriyama Y. A human transporter protein that mediates the final excretion step for toxic organic cations. Proc Natl Acad Sci U S A. 2005;102:17923–8.
10. Masuda S, Terada T, Yonezawa A, Tanihara Y, Kishimoto K, Katsura T, *et al.* Identification and functional characterization of a new human kidney-specific H+/organic cation antiporter, kidney-specific multidrug and toxin extrusion 2. J Am Soc Nephrol. 2006;17:2127–35.
11. Moriyama Y, Hiasa M, Matsumoto T, Omote H. Multidrug and toxic compound extrusion (MATE)-type proteins as anchor transporters for the excretion of metabolic waste products and xenobiotics. Xenobiotica. 2008;38:1107–18.
12. Terada T, Inui K. Physiological and pharmacokinetic roles of H+/organic cation antiporters (MATE/SLC47A). Biochem Pharmacol. 2008;75:1689–96.
13. Tanihara Y, Masuda S, Sato T, Katsura T, Ogawa O, Inui K. Substrate specificity of MATE1 and MATE2-K, human multidrug and toxin extrusions/H(+)-organic cation antiporters. Biochem Pharmacol. 2007;74:359–71.
14. Christensen MM, Pedersen RS, Stage TB, Brasch-Andersen C, Nielsen F, Damkier P, *et al.* A gene-gene interaction between polymorphisms in the OCT2 and MATE1 genes influences the renal clearance of metformin. Pharmacogenet Genomics. 2013;23(10):526–34.
15. Becker ML, Visser LE, van Schaik RH, Hofman A, Uitterlinden AG, Stricker BH. Genetic variation in the multidrug and toxin extrusion 1 transporter protein influences the glucose-lowering effect of metformin in patients with diabetes: a preliminary study. Diabetes. 2009;58:745–9.
16. Stocker SL, Morrissey KM, Yee SW, Castro RA, Xu L, Dahlin A, *et al.* The effect of novel promoter variants in MATE1 and MATE2 on the pharmacokinetics and pharmacodynamics of metformin. Clin Pharmacol Ther. 2013;93(2):186–94.
17. Tsuda M, Terada T, Ueba M, Sato T, Masuda S, Katsura T, *et al.* Involvement of human multidrug and toxin extrusion 1 in the drug interaction between cimetidine and metformin in renal epithelial cells. J Pharmacol Exp Ther. 2009;329(1):185–91.
18. Grun B, Kiessling MK, Burhenne J, Riedel KD, Weiss J, Rauch G, *et al.* Trimethoprim-metformin interaction and its genetic modulation by OCT2 and MATE1 transporters. Br J Clin Pharmacol. 2013;76(5):787–96.
19. Watanabe T, Kusuhara H, Sugiyama Y. Application of physiologically based pharmacokinetic modeling and clearance concept to drugs showing transporter-mediated distribution and clearance in humans. J Pharmacokinet Pharmacodyn. 2010;37:575–90.
20. Kusuhara H. Imaging in the study of membrane transporters. Clin Pharmacol Ther. 2013;94:33–6.
21. Ijuin R, Takashima T, Watanabe Y, Sugiyama Y, Suzuki M. Synthesis of [11C]dehydropravastatin, a PET probe potentially useful for studying OATP1B1 and MRP2 transporters in the liver. Bioorg Med Chem. 2012;20:3703–9.
22. Shingaki T, Takashima T, Ijuin R, Zhang X, Onoue T, Katayama Y, *et al.* Evaluation of oatp and Mrp2 activities in hepatobiliary excretion using newly developed positron emission tomography (PET) tracer, [11C]dehydropravastatin, in rats. J Pharmacol Exp Ther. 2013;347:193–202.
23. Takashima T, Nagata H, Nakae T, Cui Y, Wada Y, Kitamura S, *et al.* Positron emission tomography studies using (15R)-16-m-[11C]tolyl-17,18,19,20-tetranorisocarbacyclin methyl ester for the evaluation of hepatobiliary transport. J Pharmacol Exp Ther. 2010;335:314–23.
24. Takashima T, Kitamura S, Wada Y, Tanaka M, Shigihara Y, Ishii H, *et al.* PET imaging-based evaluation of hepatobiliary transport in humans with (15R)-11C-TIC-Me. J Nucl Med. 2012;53:741–8.
25. Takashima T, Hashizume Y, Katayama Y, Murai M, Wada Y, Maeda K, *et al.* The involvement of organic anion transporting polypeptide in the hepatic uptake of telmisartan in rats: PET studies with [11C]telmisartan. Mol Pharm. 2011;8:1789–98.
26. Takashima T, Wu C, Takashima-Hirano M, Katayama Y, Wada Y, Suzuki M, *et al.* Evaluation of breast cancer resistance protein function in hepatobiliary and renal excretion using PET with 11C-SC-62807. J Nucl Med. 2013;54:267–76.
27. Takashima T, Yokoyama C, Mizuma H, Yamanaka H, Wada Y, Onoe K, *et al.* Developmental changes in P-glycoprotein function in the blood–brain barrier of nonhuman primates: PET study with R-11C-verapamil and 11C-oseltamivir. J Nucl Med. 2011;52:950–7.
28. Hume WE, Shingaki T, Takashima T, Watanabe Y. The synthesis and biodistribution of [11C]metformin as a PET probe to study hepatobiliary transport mediated by the multi-drug and toxin extrusion transporter 1 (MATE1) in vivo. Bioorg Med Chem. 2013;21:7584–90.
29. Davies B, Morris T. Physiological parameters in laboratory animals and humans. Pharm Res. 1993;10:1093–5.
30. Tsuda M, Terada T, Mizuno T, Katsura T, Shimakura J, Inui K. Targeted disruption of the multidrug and toxin extrusion 1 (mate1) gene in mice reduces renal secretion of metformin. Mol Pharmacol. 2009;75:1280–6.
31. Zamek-Gliszczynski MJ, Hoffmaster KA, Tweedie DJ, Giacomini KM, Hillgren KM. Highlights from the international transporter consortium second workshop. Clin Pharmacol Ther. 2012;92(5):553–6.
32. Nakamura T, Yonezawa A, Hashimoto S, Katsura T, Inui K. Disruption of multidrug and toxin extrusion MATE1 potentiates cisplatin-induced nephrotoxicity. Biochem Pharmacol. 2010;80:1762–7.
33. Ito S, Kusuhara H, Yokochi M, Toyoshima J, Inoue K, Yuasa H, *et al.* Competitive inhibition of the luminal efflux by multidrug and toxin extrusions, but not basolateral uptake by organic cation transporter 2, is the likely mechanism underlying the pharmacokinetic drug-drug interactions caused by cimetidine in the kidney. J Pharmacol Exp Ther. 2012;340:393–403.
34. Somogyi A, Stockley C, Keal J, Rolan P, Bochner F. Reduction of metformin renal tubular secretion by cimetidine in man. Br J Clin Pharmacol. 1987;23:545–51.